AGU PUBLICATIONS

JGR

Journal of Geophysical Research: Atmospheres

RESEARCH ARTICLE
10.1002/2013JD021099

Key Points:
- North African dust is studied using observations and models
- Observations agree in the magnitude, distribution, and seasonality of dust
- Models show large differences to observations and they show large diversity

Supporting Information:
- Readme
- Table S1
- Figure S1
- Figure S2
- Figure S3

Correspondence to:
D. Kim,
dongchul.kim@nasa.gov

Citation:
Kim, D., et al. (2014), Sources, sinks, and transatlantic transport of North African dust aerosol: A multimodel analysis and comparison with remote sensing data, *J. Geophys. Res. Atmos.*, *119*, 6259–6277, doi:10.1002/2013JD021099.

Received 28 OCT 2013
Accepted 1 MAY 2014
Accepted article online 6 MAY 2014
Published online 28 MAY 2014

Sources, sinks, and transatlantic transport of North African dust aerosol: A multimodel analysis and comparison with remote sensing data

Dongchul Kim[1,2], Mian Chin[2], Hongbin Yu[2,3], Thomas Diehl[1,2], Qian Tan[1,2], Ralph A. Kahn[2], Kostas Tsigaridis[4,5], Susanne E. Bauer[4,5], Toshihiko Takemura[6], Luca Pozzoli[7], Nicolas Bellouin[8], Michael Schulz[9], Sophie Peyridieu[10], Alain Chédin[10], and Brigitte Koffi[11]

[1]Universities Space Research Association, Columbia, Maryland, USA, [2]Earth Sciences Division, NASA Goddard Space Flight Center, Greenbelt, Maryland, USA, [3]Earth System Sciences Interdisciplinary Center, University of Maryland, College Park, Maryland, USA, [4]Center for Climate Systems Research, Columbia University, New York, New York, USA, [5]NASA Goddard Institute for Space Studies, New York, New York, USA, [6]Research Institute for Applied Mechanics, Kyushu University, Fukuoka, Japan, [7]Eurasia Institute of Earth Sciences, Istanbul Technical University, Istanbul, Turkey, [8]Met Office Hadley Centre, Exeter, UK, [9]Norwegian Meteorological Institute, Oslo, Norway, [10]Laboratoire de Météorologie Dynamique, Palaiseau, France, [11]Institute for Environment and Sustainability, Air and Climate Unit, Joint Research Center, European Commission, Ispra, Italy

Abstract This study evaluates model-simulated dust aerosols over North Africa and the North Atlantic from five global models that participated in the Aerosol Comparison between Observations and Models phase II model experiments. The model results are compared with satellite aerosol optical depth (AOD) data from Moderate Resolution Imaging Spectroradiometer (MODIS), Multiangle Imaging Spectroradiometer (MISR), and Sea-viewing Wide Field-of-view Sensor, dust optical depth (DOD) derived from MODIS and MISR, AOD and coarse-mode AOD (as a proxy of DOD) from ground-based Aerosol Robotic Network Sun photometer measurements, and dust vertical distributions/centroid height from Cloud Aerosol Lidar with Orthogonal Polarization and Atmospheric Infrared Sounder satellite AOD retrievals. We examine the following quantities of AOD and DOD: (1) the magnitudes over land and over ocean in our study domain, (2) the longitudinal gradient from the dust source region over North Africa to the western North Atlantic, (3) seasonal variations at different locations, and (4) the dust vertical profile shape and the AOD centroid height (altitude above or below which half of the AOD is located). The different satellite data show consistent features in most of these aspects; however, the models display large diversity in all of them, with significant differences among the models and between models and observations. By examining dust emission, removal, and mass extinction efficiency in the five models, we also find remarkable differences among the models that all contribute to the discrepancies of model-simulated dust amount and distribution. This study highlights the challenges in simulating the dust physical and optical processes, even in the best known dust environment, and stresses the need for observable quantities to constrain the model processes.

1. Introduction

Dust contributes about 70% of global aerosol mass and one quarter of the total aerosol optical depth in midvisible wavelengths [e.g., *Kinne et al.*, 2006]. Dust plays an important role in global climate by interacting with solar and terrestrial radiation, altering cloud amount and radiative properties [*Haywood et al.*, 2003; *Forster et al.*, 2007; *Evan et al.*, 2008; *Kim et al.*, 2010; *Zhao et al.*, 2011], and fertilizing land and ocean, and hence modulating carbon uptake [*Jickells et al.*, 2005; *Maher et al.*, 2010]. The impact of dust can go well beyond desert regions, on hemispheric or even global scales [*Carlson and Prospero*, 1972; *Prospero*, 1999; *Kaufman et al.*, 2005; *Uno et al.*, 2009; *Yu et al.*, 2012]. Thus, the dust cycle is an integral part of the Earth system, and it has become an emerging core theme in Earth system science [*Shao et al.*, 2011].

North Africa is the largest dust source region in the world [e.g., *Prospero et al.*, 2002]. The emission, transport, and deposition of North African dust are strongly influenced by meteorology, resulting in strong seasonal variability and multidecadal oscillation [*Mahowald*, 2007; *Mahowald et al.*, 2010]. Significant correlations exist between dust and climate variables, such as sea surface temperature, the North Atlantic Oscillation, and the Madden-Julian Oscillation [e.g., *Ginoux et al.*, 2004; *Wong et al.*, 2008; *Guo et al.*, 2013]. However, modeling of North African dust cycles and the impacts remains challenging for global or regional numerical models, as the complex

Table 1. Description of the Participating Models and Their Dust Physical Characteristics

	GOCART	GISS-ModelE	SPRINTARS	ECHAM5-HAMMOZ[a]	HadGEM2
Resolution	2.5° × 2°	2.5° × 2°	1.125° × 1.125°	2.8° × 2.8°	1.875° × 1.25°
Vertical layers	30	40	56	31	38
Meteorology	GEOS4 DAS	Horizontal winds nudged to NCEP Reanalysis	NCEP Reanalysis	ECMWF Reanalysis	ECMWF Reanalysis
Winds for emissions	U_{10m}^3	U_{10m}^3	U_{10m}^3	U_*^3	U_*^3
Size distribution (μm)	Five bins 0.1-1.0-1.8-3.0-6.0-10.0	Five bins 0.1-1-2-4-8-16	Six bins 0.1-0.22-0.46-1.0-2.15-4.64-10.0	Two modes (acc. and coarse) $0.05 < r_m < 0.5$ $0.5 < r_m$	Six bins 0.0316-0.1-0.316-1.0-3.16-10-31.6
Density (g m^3)	2.5	2.5 for clay 2.65 for silt	2.6	2.5–2.6	2.65
Major references	*Chin et al.* [2002, 2009] and *Ginoux et al.* [2001]	*Miller et al.* [2006] and *Bauer and Koch* [2005]	*Takemura et al.* [2000, 2005]	*Pozzoli et al.* [2008, 2011]	*Bellouin et al.* [2011, Appendix A]

[a]Dust particles are emitted in the insoluble accumulation and coarse modes with mass median radii of 0.37 μm and 1.75 μm, respectively. Once emitted, dust particles can be mixed with other aerosols, and dust is distributed in two additional modes: internally mixed soluble accumulation and coarse modes.

dust processes are often parameterized with a suite of simplifications [e.g., *Tegen and Fung*, 1995; *Guelle, et al.*, 2000; *Ginoux et al.*, 2001; *Zender et al.*, 2003; *Nowottnick et al.*, 2010; *Huneeus et al.*, 2011; *Ridley et al.*, 2012]. For example, evaluation of multiple global models participating in the Aerosol Comparison between Observations and Models (AeroCom) phase I experiments showed large discrepancies in dust emissions, horizontal and vertical distribution, transported particle size, deposition, and lifetimes among models or between models and observations [*Textor et al.*, 2006; *Huneeus et al.*, 2011; *Koffi et al.*, 2012; *Prospero et al.*, 2010]. Although most models were able to reproduce the transatlantic dust transport pattern, they differ in magnitude and seasonality, and in general, models perform better in summer than in winter over the Atlantic [*Huneeus et al.*, 2011]. Comparisons of aerosol vertical distributions of AeroCom I models with satellite observations from the Cloud Aerosol Lidar with Orthogonal Polarization (CALIOP) revealed inconsistencies, i.e., aerosol effective height from the models was generally lower over North African source regions but higher over the Atlantic than that from CALIOP observations [*Koffi et al.*, 2012]. A previous study also found large differences in dry and wet deposition of dust between the AeroCom I models and measurements over Florida [*Prospero et al.*, 2010].

Complementary to the previous studies, this study examines the performance of models that participated in the Hindcast experiment in the second phase of the AeroCom study (AeroCom II). We focus on the AeroCom II model simulations of the North African dust and its transatlantic transport from 2000 to 2005, evaluate the simulated dust amounts, spatial distributions, and seasonal and interannual variability using satellite and ground-based remote sensing data, and examine several key physical and optical parameters among the models that may help diagnose model behavior. The main objective of this paper is to assess the model simulations of dust in the best known dust environment.

In section 2, we briefly describe the AeroCom phase II Hindcast model simulations and the satellite- and ground-based remote sensing measurements. In section 3, we compare the observed and modeled total aerosol and dust aerosol optical depths, including their longitudinal gradients, multiyear variations, and vertical distributions. We then investigate the differences among the models by examining several physical and optical properties in dust simulations in section 4. Discussion and summary are presented in sections 5 and 6, respectively.

2. Models and Data

2.1. AeroCom Models

The AeroCom initiative is an internationally coordinated effort to advance the understanding of atmospheric aerosols and their environmental impacts through organized multimodel experiments and to document and diagnose differences among models and between models and observations (http://aerocom.met.no). Built upon the success of Phase I activities [*Textor et al.*, 2006; *Kinne et al.*, 2006; *Schulz et al.*, 2006], AeroCom phase II experiments and activities were designed to further quantify and reduce the uncertainty in aerosol climate forcing estimates. In this study, we use global aerosol models in the AeroCom phase II Hindcast experiments that produced multiyear simulations from 1980 to the 2000s. Five models that submitted dust diagnostics were selected for this study, with dust simulation characteristics summarized in Table 1. We analyze the results over the time period of 2000–2005, due to the availability of both validation data and multiple model output.

Table 2. Remote Sensing Data Used in This Study

Sensor/Platform	Data Products	Major References
MODIS	AOD (dark target + deep blue)	*Levy et al.* [2010], *Hsu et al.* [2004]
	DOD derived from AOD and coarse-mode fraction over ocean	*Yu et al.* [2009], and *Kaufman et al.* [2005]
MISR	AOD	*Kahn et al.* [2010]
	DOD derived from AOD and nonspherical fraction	*Kalashnikova and Kahn* [2006]
SeaWiFS	AOD	*Sayer et al.* [2012] and *Hsu et al.* [2012]
CALIOP	Extinction profile for dust	*Koffi et al.* [2012]
AIRS	Dust centroid height (nighttime and over ocean)	*Peyridieu et al.* [2010, 2013]
AERONET	AOD, coarse-mode AOD	*Holben et al.* [1998] and *Dubovik et al.* [2000]

We compare several monthly mean fields from the model output, namely the total aerosol optical depth (AOD), dust optical depth (DOD), dust mass loading (LOAD), emission (EMI), dry deposition (DRY), wet deposition (WET), and total precipitation. In addition, we analyze several physical and optical properties derived from the standard monthly outputs to sort out potential reasons for the model-model and model-observation differences.

The model setup and configurations are model dependent, with a horizontal resolution from 1.1° to 2.8°. The input meteorology fields that drive dust emissions and transport are taken from three reanalysis products, namely, NCEP (used by GISS-ModelE, hereafter GISS, and SPRINTARS), ECMWF (used by ECHAM5-HAMMOZ, hereafter ECHAM5, and HadGEM2), and GEOS4 (used by GOCART). Some models use 10 m wind for dust mobilization parameterization (GOCART, GISS, and SPRINTARS), whereas others use friction velocity (u_*). The models also differ in dry and wet deposition parameterizations and source locations, but they all consider sedimentation and turbulence in the dry deposition scheme, as well as rainout (in-cloud) and washout (below-cloud) by convective and large-scale precipitation in the wet deposition scheme. Although dust density values are similar among the models, the number and range of dust size groups are quite different, from two modes with size range of 0.05–0.5 μm (radius) in ECHAM5 to six bins with size range of 0.03–31.6 μm (radius) in HadGEM2 (Table 1). The size differences will affect dust emission mass, transport, deposition, and loading, as well as the average extinction efficiency in different models [*Zhao et al.*, 2010, 2013; *Mahowald et al.*, 2013].

Although AOD and DOD from remote sensing products used in this study are limited to clear-sky scenes [*Kahn et al.*, 2010; *Levy et al.*, 2010], model outputs are only available for all-sky conditions except the GISS model, which provides values for both all-sky (GISS_AS, AOD_AS and DOD_AS) and clear-sky conditions (GISS_CS, AOD_CS and DOD_CS); both are used in this study. Although the clear-sky results are more appropriate for comparisons with satellite observations, the all-sky results are used for intermodel comparisons because most models do not have the clear-sky-only results. Note that heterogeneous chemistry (i.e., condensation of sulfate and nitrate on dust surfaces) in the GISS model will affect wet deposition, as coated dust particles are more soluble [*Bauer and Koch*, 2005]. However, the mixing state does not affect to the optical calculation [*Bauer et al.*, 2007]. The ECHAM5 model considers four soluble modal size bins as internal mixtures of aerosol components and three insoluble modal size bins, an internal mixture of organic carbon and black carbon in the Aitken mode, and externally mixed dust particles in the accumulation and coarse modes (M7, *Vignati et al.* [2004]). ECHAM5 calculates AOD for each mode using the volume-weighted average of the refractive indices of the different aerosol components, including the diagnosed aerosol water [*Stier et al.*, 2005]. Thus, in ECHAM5 only an approximation of DOD can be calculated as the sum of the AOD of two externally mixed dust modes and the dust volume-weighted AOD of two internally mixed modes where dust is present. This approach may cause additional differences between ECHAM5 and other models in the intermodel comparison.

2.2. Remote Sensing Data

Several observational data sets (listed in Table 2) are used to evaluate the model simulations. Seasonal and spatial distributions of AOD are taken from the Moderate Resolution Imaging Spectroradiometer (MODIS) onboard the Terra satellite (collection 5.1) [*Hsu et al.*, 2006; *Levy et al.*, 2010], the Multiangle Imaging Spectroradiometer (MISR) [*Kahn et al.*, 2010], and the Sea-viewing Wide Field-of-view Sensor (SeaWiFS) [*Sayer et al.*, 2012; *Hsu et al.*, 2012]. The MODIS deep-blue AOD retrieved over bright deserts [*Hsu et al.*, 2004] is

used to fill the gaps in the "standard" MODIS dark target retrievals [*Levy et al*., 2010]. In addition to total AOD, we also use dust optical depth (DOD) over ocean derived from the MODIS and MISR retrievals of AOD and particle properties (e.g., size and shape). MODIS AOD over ocean and fine-mode fraction (f) measurements have been used to empirically separate AOD of dust (du) from that of combustion or anthropogenic (an, as referred to in some studies) and marine (ma) aerosol in a self-consistent way [*Kaufman et al*., 2005; *Yu et al*., 2009]. Given that $\tau = \tau_{ma} + \tau_{du} + \tau_{an}$ and $f = [f_{ma}\tau_{ma} + f_{du}\tau_{du} + f_{an}\tau_{an}]/\tau$, DOD ($\tau_{du}$) is derived from MODIS Collection 5.1 data using representative values for f_{ma}, f_{du}, f_{an}, and τ_{ma} derived specifically for the transatlantic dust transport from North Africa [*Yu et al*., 2009]. For MISR we use the nonspherical AOD fraction (i.e., ns-AOD) as equivalent to DOD [*Kalashnikova and Kahn*, 2006; *Kahn et al*., 2009; *Guo et al*., 2013]. DOD retrieval is available only over ocean for MODIS and is generally of higher quality over ocean for MISR, due to the large uncertainties of the required parameters over land.

To evaluate the vertical distribution of dust, we use the dust aerosol extinction profiles from CALIOP, archived in the AeroCom data server. The CALIOP product is the gridded monthly global data with $1° \times 1°$ horizontal resolution and 100 m vertical resolution [*Koffi et al*., 2012]. It includes mean extinction profiles of total and dust aerosol as derived from CALIOP Layer v3.01 data. Dust has been identified using the threshold volume depolarization ratio ($>$0.06), following previous studies [*Liu et al*., 2008; *Yu et al*., 2010]. Like *Koffi et al*. [2012], we only use nighttime CALIOP extinction profiles, due to their better data quality and availability. *Koffi et al*. [2012] showed their 2007–2009 CALIOP-gridded product to provide consistent mean regional and seasonal patterns of the aerosol vertical distribution over North Africa and over the Atlantic, together with a low interannual variability. The uncertainty of AOD of CALIOP is less than 10% of the MODIS AOD over the Atlantic. The CALIOP aerosol extinction vertical profiles are 0.003 km^{-1} (~20%) and 0.15 km^{-1} (~50%) higher than High Spectral Resolution Lidar measurements over U.S. and Gulf of Mexico, respectively [*Omar et al*., 2009]. We use dust AOD centroid height from the Atmospheric Infrared Sounder (AIRS) nighttime measurements over ocean [*Peyridieu et al*., 2010, 2013]. Here the AOD centroid height is defined as the altitude above or below which half the total-column AOD is located. The AIRS senses atmospheric aerosols with a thermal infrared channel at 10 μm wavelength, in the atmospheric window, which is most sensitive to dust aerosol. All satellite remote sensing data have been extensively validated against surface-based Aerosol Robotic Network (AERONET) measurements over various time and regions (see references in Table 2 for detailed validation result of the satellite AOD).

We also use total AOD and coarse-mode AOD (Version 2, Level 1.5 and 2) from ground-based Aerosol Robotic Network (AERONET) [*Holben et al*., 1998] sites located within the study domain to evaluate both satellite measurements and model simulations. There are eight AERONET sites in the study region, including three inland sites (Agoufou, Banizoumbou, and Ouagadougou) in North Africa, two coastal sites (Dahkla and Dakar) in the western part of North Africa, two island sites (Cape Verde and La Parguera) in the North Atlantic, and one coastal site in South America (Surinam) (see Figure 5 for latitude and longitude coordinates of these sites). The ground-based observations over dust source regions and the transatlantic transport route can offer important insights into the evolution of North African dust on the intercontinental scale. In particular, La Parguera, situated in the Caribbean Sea, is about 4000 km downwind of Cape Verde near the African coast, providing a benchmark for characterizing the Saharan dust transatlantic transport at a receptor location.

All the model-data comparisons are performed on either a monthly, seasonal, or multiyear average basis, i.e., without matching satellite overpass time and AERONET sampling time or considering missing data on some days. This approach might introduce some artifacts in the observed differences between model and data, but, given the large amount of available data, over a 6 year time span, it should not affect our statistics and conclusions.

3. Comparisons of Model Simulations With Satellite and Ground-Based Measurements

The domain of this study (90°W ~ 30°E; 0°N ~ 35°N) covers most dust source regions in North Africa, plus the transatlantic transport route (referred to as the DOMAIN). The domain consists of North Africa (LAND, 17°W ~30°E; 0°N ~ 35°N) and the North Atlantic Ocean (OCEAN, 90°W ~ 17°W; 0°N ~ 35°N) (see Figure 1). We evaluate the model results with remote sensing data by comparing the mean AOD and DOD in the study domain (section 3.1), the longitudinal gradient from the dust source region in North Africa to the western North Atlantic (section 3.2), the seasonal variations of AOD and DOD at different geographic locations (section 3.3), and the vertical distribution and centroid height of dust over land and ocean (section 3.4).

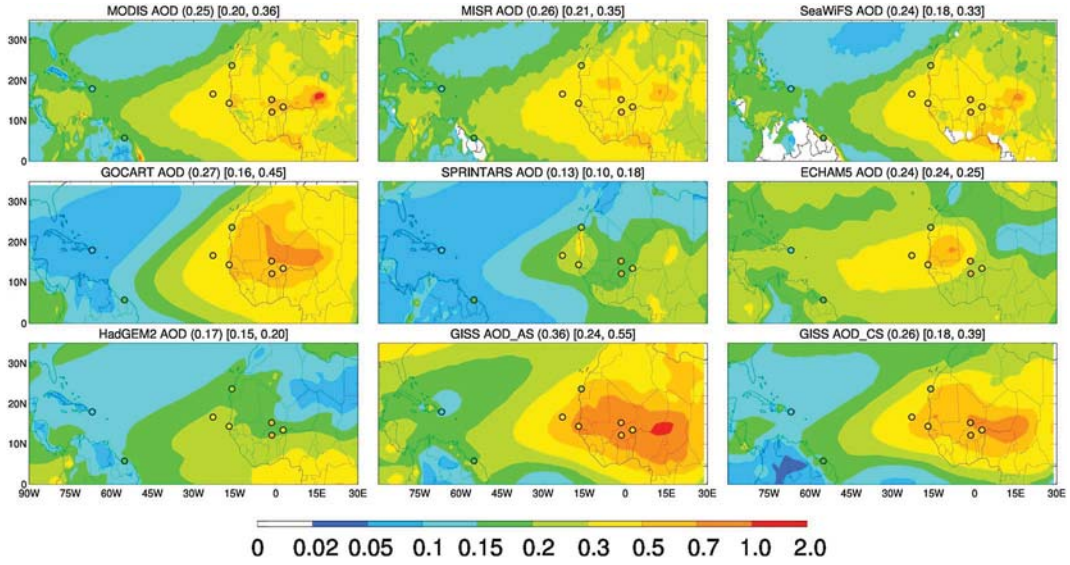

Figure 1. Spatial distribution of mean total AOD from satellites (MODIS, MISR, and SeaWiFS) and models (GOCART, SPRINTARS, ECHAM5, HadGEM2, and GISS) averaged from 2000 to 2005. Color circles superimposed on the map represent AERONET observed AOD. Number in parentheses is the mean of whole domain, and numbers in brackets are the mean of ocean and land, respectively. AOD_AS and AOD_CS in GISS represent all-sky and clear-sky AOD, respectively.

3.1. Mean AOD and DOD

Figure 1 shows a comparison between satellite observations and model simulations of the 6 year mean total AOD averaged from 2000 to 2005, with AERONET AODs at eight sites superimposed using the same color scale. MODIS, MISR, and SeaWiFS agree on the domain average (0.25, 0.26, and 0.24, respectively), with about 0.35 over land and 0.20 over ocean. The AOD decreases by a factor of 2 ~ 3 from the coast of North Africa westward to the Caribbean Sea, presumably because of dry and wet removal during transport, along with some horizontal dilution. The satellites agree with AERONET AOD to within 20–40% at most locations despite differences in spatial and temporal sampling. However, the multiyear mean AODs from the models differ considerably, by ranging from 0.13 (SPRINTARS) to 0.36 (GISS_AS) over the domain, 0.18 (SPRINTARS) to 0.55 (GISS_AS) over land, and 0.10 (SPRINTARS) to 0.24 (GISS_AS, ECHAM5) over ocean. As shown in Table 3, GOCART and GISS_CS better capture the magnitude of satellite-retrieved AOD over both land and ocean than other models do, although the land-ocean gradient from GOCART is too strong (we discuss the longitudinal gradient in next section). AOD from SPRINTARS and HadGEM2 are considerably lower than the satellite products over both land and ocean, whereas ECHAM5 AOD is higher over ocean but lower over land compared to the satellite observations.

Similar to AOD, the mean distributions of satellite-derived DOD from MODIS and MISR agree reasonably well, with OCEAN average values of 0.12 and 0.10, respectively (Figure 2). The satellite-derived annual mean DODs are about half the corresponding AODs on average, suggesting that nondust aerosols contribute about 50% to AOD on annual and domain basis over the North Atlantic. The AERONET coarse-mode AOD values at Cape Verde and La Parguera are about 0.05 and 0.1 higher than the corresponding DOD values from MODIS and MISR, respectively, but especially at La Parguera, coarse-mode sea salt can contribute to the AERONET value. The distribution patterns of modeled DOD are similar to their AODs, i.e., high DOD values over land and rapid decreases off the coast. Again, there is a large diversity among the models in simulated DOD. The multiyear domain-averaged DOD from the models falls within the range of 0.04 (HadGEM2) to 0.17 (GOCART), i.e., differing by a factor of ~4, which is almost twice as large as the range of AOD. The model-calculated mean DOD over ocean ranges from 0.03 to 0.09, consistently smaller than the satellite-derived DOD over ocean (0.10–0.12). Similar to the satellites, DODs from all models are lower than the coarse-mode AOD from AERONET at La Parguera by 0.08–0.1.

Table 3. Mean of Standard Physical and Optical Model Outputs Over Different Domains[a]

	Name	Unit	GOCART	GISS[b]	SPRINTARS	ECHAM5	HadGEM2	Diversity (%)
Domain (90°W–30°E, 0°N–35°N)	EMI	Tg yr^{-1}	2025	1087	791	422	914	57.1
	DRY	Tg yr^{-1}	1430	680	675	189	781	59.1
	WET	Tg yr^{-1}	357	266	99	151	85	60.8
	LOAD	Tg	17.1	10.7	3.9	5.4	4.0	69.3
	DOD	Unitless	0.17	0.15 (0.14)	0.07	0.06	0.04	59.0
	AOD	Unitless	0.27	0.36 (0.26)	0.13	0.24	0.17	38.0
	f_{DOD}	Fraction	0.48	0.27 (0.35)	0.39	0.20	0.23	38.6
	f_{WET}	Fraction	0.47	0.63	0.36	0.48	0.58	21.0
	LF	day^{-1}	0.28	0.37	0.34	0.31	0.35	10.8
	MEE	$m^2\ g^{-1}$	0.60	0.76	1.05	0.56	0.64	27.4
Land (17°W–30°E, 0°N–35°N)	DRY	Tg yr^{-1}	1256	602	595	134	755	59.8
	WET	Tg yr^{-1}	182	148	74	48	41	63.4
	LOAD	Tg	12.5	8.0	2.7	3.1	2.6	74.8
	DOD	Unitless	0.33	0.29 (0.29)	0.12	0.11	0.06	65.8
	AOD	Unitless	0.45	0.55 (0.39)	0.18	0.25	0.20	50.3
	f_{DOD}	Fraction	0.68	0.46 (0.61)	0.60	0.34	0.35	31.1
	f_{WET}	Fraction	0.27	0.39	0.28	0.31	0.33	15.3
	LF	day^{-1}	0.29	0.29	0.53	0.22	0.61	44.0
	MEE	$m^2\ g^{-1}$	0.52	0.69	0.93	0.60	0.49	26.9
Ocean (90°W–17°W, 0°N–35°N)	DRY	Tg yr^{-1}	174	78	80	55	26	67.3
	WET	Tg yr^{-1}	175	118	25	103	44	64.9
	LOAD	Tg	4.7	2.7	1.2	2.3	1.4	56.5
	DOD	Unitless	0.09	0.07 (0.07)	0.04	0.05	0.03	44.8
	AOD	Unitless	0.16	0.24 (0.18)	0.10	0.24	0.15	33.6
	f_{DOD}	Fraction	0.40	0.17 (0.22)	0.28	0.12	0.15	50.2
	f_{WET}	Fraction	0.58	0.77	0.41	0.59	0.75	23.4
	LF	day^{-1}	0.28	0.42	0.22	0.37	0.16	37.1
	MEE	$m^2\ g^{-1}$	0.64	0.79	1.13	0.54	0.72	29.3

[a]Diversity of model parameters (%) is defined as the ratio of standard deviation to the mean of a parameter following *Textor et al.* [2006]. Model optical depths are all sky, unless noted otherwise.
[b]Numbers in the parentheses are clear-sky values.

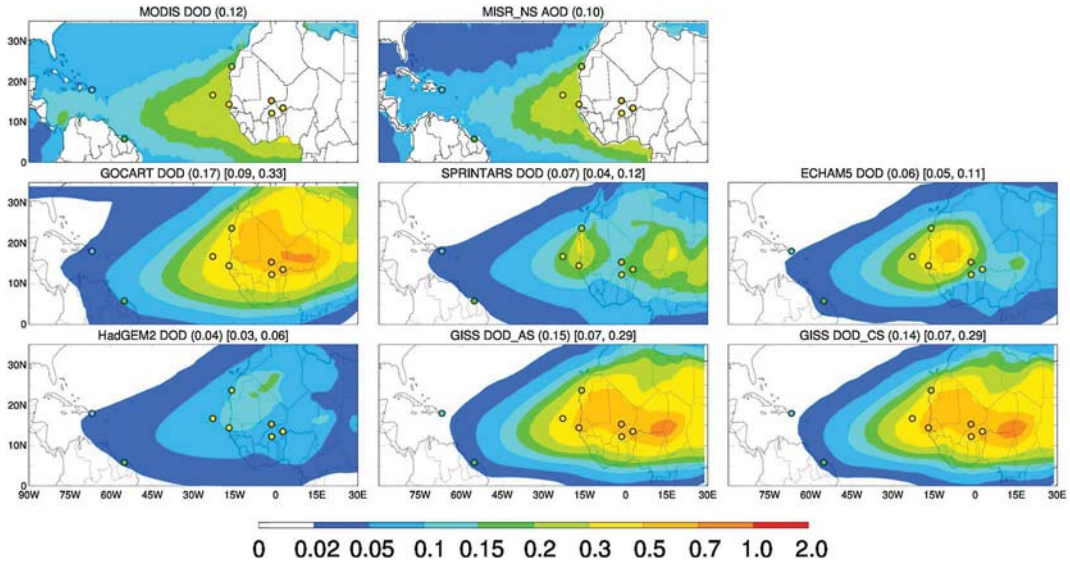

Figure 2. Spatial distributions of mean dust optical depth (DOD) from satellites (MODIS and MISR) and models (GOCART, SPRINTARS, ECHAM5, HadGEM2, and GISS) averaged from 2000 to 2005. MODIS DOD is derived from a method described in *Yu et al.* [2009], and MISR nonspherical AOD represents DOD. Color circles superimposed on the map are the AERONET-retrieved coarse-mode AOD. For the models, number in parentheses is the mean of whole domain and numbers in brackets are the mean of ocean and land, respectively. DOD_AS and DOD_CS in GISS represent all-sky and clear-sky DOD, respectively.

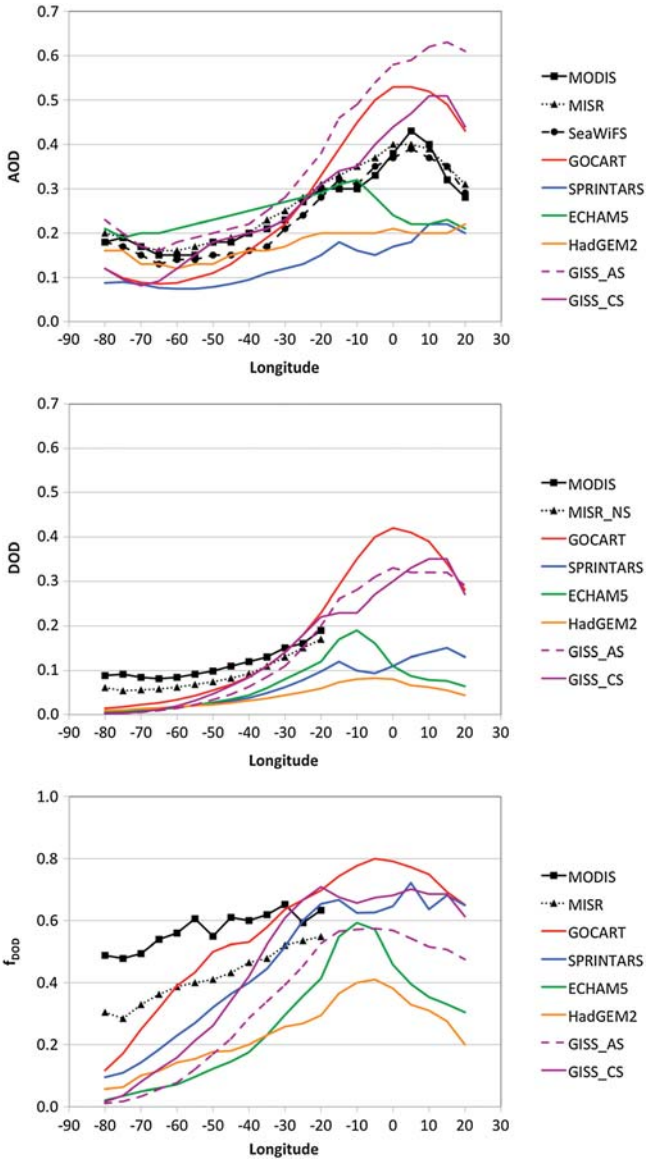

Figure 3. Meridional mean of AOD, DOD, and f_{DOD} averaged from 0 to 35°N. No DOD available from satellite-based products over land.

The clear-sky AOD (i.e., AOD_CS) from GISS shows a somewhat different distribution pattern and magnitude than the all-sky values (i.e., AOD_AS) (Figure 1). The AOD_CS is about 25% and 29% lower than the AOD_AS over ocean and land, respectively, yielding closer agreement with the satellite retrievals, that are also under clear-sky conditions only. The large difference in AOD_AS and AOD_CS is caused by the higher relative humidity (RH) in all-sky that makes hydrophilic aerosol particles, such as sea spray, ammonium sulfate and nitrate, and organic aerosols, grow larger in size and become more efficient in light extinction. As expected, DOD_CS from GISS is very close to DOD_AS throughout the domain, because dust aerosols are assumed to be hydrophobic, so RH has little effect on the extinction efficiency.

3.2. Longitudinal Gradient

As we showed in the previous section and Figures 1 and 2, the longitudinal gradients of AOD and DOD across the North Atlantic from east to west are too strong for some models. To further quantify the difference, the mean AODs from satellites and models, averaged in 5° longitude intervals between 0° and 35°N, are plotted in Figure 3 (top). The satellite AODs from MODIS, MISR, and SeaWiFS show similar magnitudes and longitudinal gradients across the domain, with a maximum value of about 0.4 between 0° and 10°E inland, and gradually decreasing across the Northern Atlantic, reaching a minimum value of about 0.15 at 60°W–65°W. The models, however, show a large diversity. GOCART captures the locations of observed AOD maximum and minimum, but it overestimates the maximum and underestimates the minimum values by 0.1 (or 25% and 100%, respectively), suggesting that the dust emission is probably too high and removal rates during transport may be too strong. GISS_CS simulates a peak AOD that is about 25% higher and shifted about 10° eastward compared to observation, but it captures the AOD gradient across the ocean. In contrast, AODs from the remaining three models, SPRINTARS, ECHAM5, and HadGEM2, are only about half the observed values east of 10°E and show much weaker land-ocean gradients. In particular, ECHAM5 displays a peak AOD near the coast and overestimates AOD over ocean by 50%, despite the low value over land.

A similar pattern is shown in the satellite-derived DOD from MODIS and MISR data over ocean (Figure 3 (middle)). DOD from MODIS is consistently higher than MISR by about 0.01–0.02, resulting in a DOD fraction ($f_{DOD,}$ Figure 3 (bottom)) from MODIS that is higher than that from MISR by 0.1–0.2. Although the GOCART and GISS models agree with satellite-derived DOD within 25% in the coastal area (~20°W), SPRINTARS, ECHAM5, and HadGEM2 are

factors of 2–5 lower at the same location. Similar to the AOD case, GOCART has a stronger but HadGEM2 has a weaker DOD gradient across the ocean than the satellite data. Unlike AOD, all the models substantially underestimate DOD west of 50°W. The satellite-derived DOD fraction, f_{DOD}, shows a 0.1–0.15 decrease from east to west of the North Atlantic, in contrast to the much larger decrease in the models, for example, a 0.5–0.6 f_{DOD} drop in GOCART and SPRINTARS and nearly 0.7 in GISS_CS. Note, however, that some cirrus contamination in the satellite-derived dust fraction over ocean might contribute to the reported DOD [e.g., *Pierce et al*., 2010], though this is unlikely to account for the entire discrepancy. Over land, the model-simulated highest f_{DOD} ranges from 0.4 (HadGEM2) to 0.8 (GOCART), with corresponding DOD values of <0.1 to >0.4, respectively (and no satellite DOD available over land for comparison).

The magnitude and the east-to-west gradient of the clear-sky AOD in the GISS model are different than the all-sky values (Figure 3). The magnitude of clear-sky AOD better agrees with the satellite observations over both land and ocean. The value of f_{DOD} under clear-sky conditions is larger than that under all-sky conditions. Furthermore, this difference is larger in the eastern Atlantic (~0.2 on 30°W) than the western Atlantic (~0.05 on 60°W). Over land, the value of f_{DOD} under clear-sky conditions is 0.2–0.3 larger than that for all-sky conditions. Note that the other models only calculate AOD in all-sky conditions. The clear-sky AOD is expected to be lower and the f_{DOD} higher, as shown by the examples in the GISS model, which could either improve or degrade the agreement with satellite AOD and f_{DOD}, depending on models and locations.

Overall, satellite data show a 50% decrease of both AOD and DOD and a 0.1–0.2 decrease of f_{DOD} across the Atlantic Ocean. Most models have a stronger east-west DOD gradient, with a faster decrease of f_{DOD} from the west coast of North Africa to the western North Atlantic by 0.3–0.6, suggesting too efficient dust removal in the models during the transatlantic transport.

3.3. Seasonal Cycle and Interannual Variability

The seasonality of multiyear and regional mean AOD and DOD are examined for the ocean (90°W–17°W; 0–35°N) and land (17°W–30°E; 0–35°N), as shown in Figure 4. The three satellite data show similar seasonal variations over the OCEAN domain, with high AOD in July and low AOD between October and January. MISR AOD is consistently the highest and SeaWiFS AOD is consistently the lowest over ocean. The MISR-SeaWiFS difference is about 0.05. Over the LAND domain, satellite data indicate that high AOD (0.35–0.5) occurs between March and August and low AOD (0.2–0.3) between October and January. There are two AOD maxima in the annual cycle from the satellite data, one in March and the other one in summer, but the timing of the summer maximum is different among the satellite data, as MODIS and SeaWiFS peak in June and MISR peaks in August; this could be related at least in part to differences in sampling, as MODIS and SeaWiFS are wide-swath instruments, whereas MISR's narrower swath observes a given location about 3–4 times less frequently. The largest difference among the satellite AOD values is in May-July when the MODIS AOD is the highest and SeaWiFS is lowest, with a difference of 0.1–0.12. The amplitude of seasonal variation (difference of the highest and lowest AOD) from the satellites is ~0.1 over OCEAN and ~0.3 over LAND. Although MODIS DOD is slightly larger than MISR DOD (by 0.02–0.04) between January and May over OCEAN, the seasonal patterns of the MODIS and MISR DOD over OCEAN have similar phase, with a maximum of 0.15 in July and a low of 0.06–0.1 in winter months. The standard deviation bars in the figure indicate stronger interannual AOD variation in spring than in other seasons.

In comparison, model simulations show substantial intermodel diversity of seasonal variations. First, the range of AODs between models is >0.2 over OCEAN and >0.4 over LAND throughout the year. Although GOCART, HadGEM2, and SPRINTARS simulate a summer maximum AOD over OCEAN, GISS_AS, GISS_CS, and ECHAM5 show an AOD peak in February-March. This may in part be attributed to too much biomass burning aerosols in GISS and ECHAM5, which peak in winter/spring in Northern Africa; however, the DOD from these two models also shows a spring peak (Figure 4 (bottom, left)). The models, except GISS_AS, generate higher AOD between March and August over LAND but with different peak months. The models also display stronger interannual variation than the satellites.

There are also differences in DOD seasonal variability between model and observation and also among the models themselves. Over OCEAN, DODs from GOCART, SPRINTARS, and HadGEM2 show a summer maximum, consistent with the observations, whereas the GISS and ECHAM5 models show a maximum in spring. Over land, DOD is not available from observations, and models show disparities in the seasonality. Whereas GISS, SPRINTARS, and HadGEM2 DODs peak in March, GOCART and ECHAM5 DODs peak in May. GOCART also

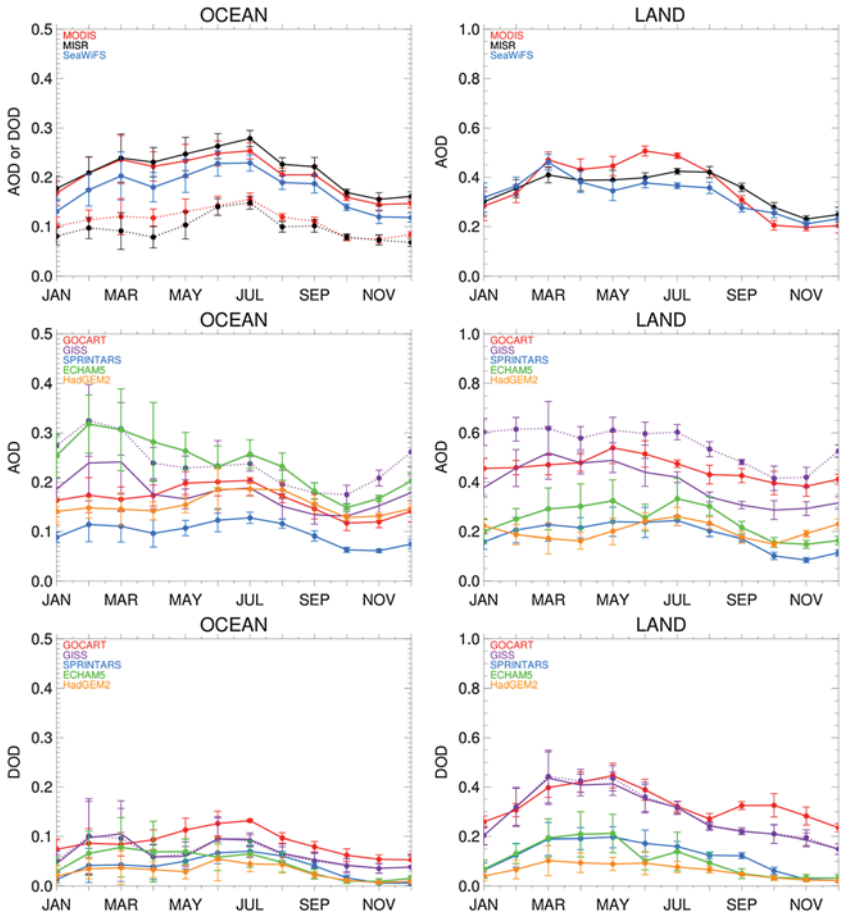

Figure 4. Monthly mean of (top) satellite AOD (solid) and DOD (dotted), (middle) model AOD, and (bottom) model DOD for ocean and land. All model plots are averaged from 2000 to 2005. Vertical bars are the standard deviation of monthly mean values. Note for different scales between LAND and OCEAN. Solid line and dotted line in GISS represent clear-sky and all-sky AOD, respectively.

shows a secondary peak in September-October. The multiyear mean (range) of modeled DOD is 0.20 (0.06–0.33) and 0.06 (0.03–0.09) over land and ocean, respectively. The relationship between modeled DOD and dust emission will be further discussed in the later sections.

Strong seasonality also appears in AOD and DOD magnitude and spatial distributions from the satellites, with a peak in June-July-August (JJA) and a minimum in December-January-February (DJF) (Figures S1 and S2 in the supporting information). The domain-averaged satellite AOD is higher in JJA (0.27–0.31) than in DJF (0.20–0.23), and the satellite DOD is higher in JJA (0.13–0.16) than in DJF (0.09–0.11). The latitudinal shifting of the dust belt by season in models agrees with the satellites, whereas models show larger ranges in JJA (0.16–0.36 for AOD; 0.06–0.19 for DOD) and in DJF (0.12–0.40 of AOD; 0.03–0.14 for DOD).

Figure 5 shows a comparison of model-simulated monthly average AOD from 2000 to 2005 with the AERONET observations at eight stations in and near the coast of North Africa and in the western Atlantic (locations indicated in Figures 1 and 2). Note that for the GISS model, only clear-sky results are shown in Figure 5 (the all-sky AOD from GISS is higher than the clear-sky AOD by a factor of 2 at La Parguera but 5–25% at other stations). The three stations at the top in the left column are in the coastal region (i.e., west of 15°W) and the three in right column are located inland (i.e., around 0°E). The AERONET AOD time series show large seasonal variability, which is much more pronounced than the regional averaged seasonal variability from satellite data. The AOD at Banizoumbou (near the dust source in the Sahel) is usually higher than that at Cape Verde (on the dust outflow route off the Western African coast) except in 2004. The time series of AERONET AOD also show large interannual variability for both the maximum and minimum values, which can differ by more than a factor of 2. Interannual

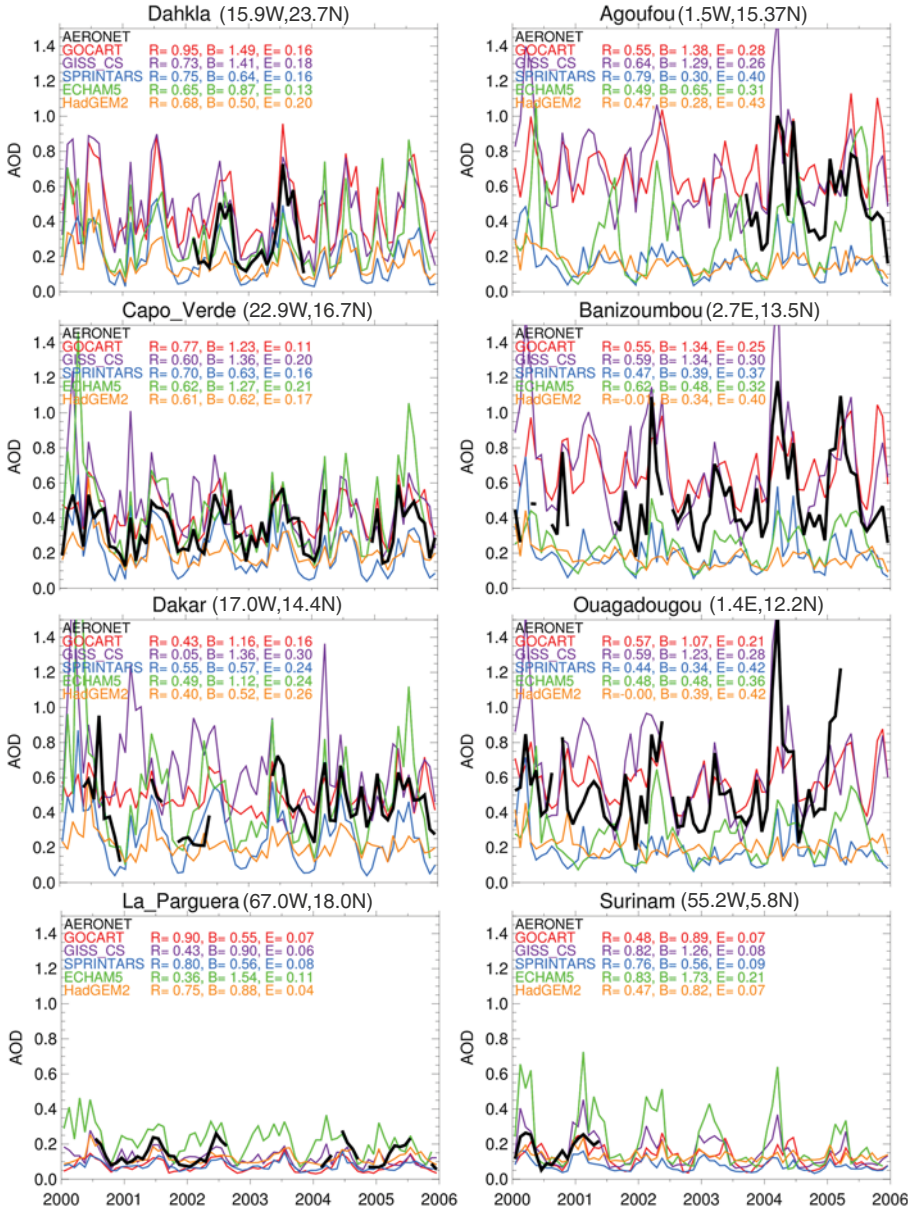

Figure 5. Comparisons of monthly mean AOD from five models (from 2000 through 2005) with AERONET measurements at six stations in North Africa and nearby islands and two stations in the western Atlantic. North Africa sites: (left) located over islands and in coastal region and (right) located inland. Numbers in the figure include correlation coefficient (*R*), mean bias (*B*), and root-mean-square error (*E*) of model AOD with respect to AERONET measurement.

AOD variations at remote AERONET stations (i.e., La Parguera and Surinam) are less than 0.1, but over source regions (i.e., Agoufou, Banizoumbou, and Ouagadougou) can be larger than 1. Model performance varies by year at all stations. Models appear to capture the summer peaks in the AERONET data; however, they show large discrepancies in overall seasonality and interannual variations.

We further measured the models' performance using the correlation coefficient (*R*), the mean bias (*B*), which is defined as the ratio of model value to observed value at each station (both values indicate better agreement with observations as they approach 1), and root-mean-square Error (*E*). *R*, *B*, and *E* values differ by model and station (Figure 5): *R* ranges from 0 (HadGEM2 at Ouagadougou) to 0.95 (GOCART at Dahkla), *B* ranges from 0.28 (HadGEM2 at Agoufou) to 1.73 (ECHAM5 at Surinam), and *E* ranges from 0.04 (HadGEM2 at La Parguera) to 0.43 (HadGEM2 at Agoufou). The decreasing longitudinal AOD gradient between the source

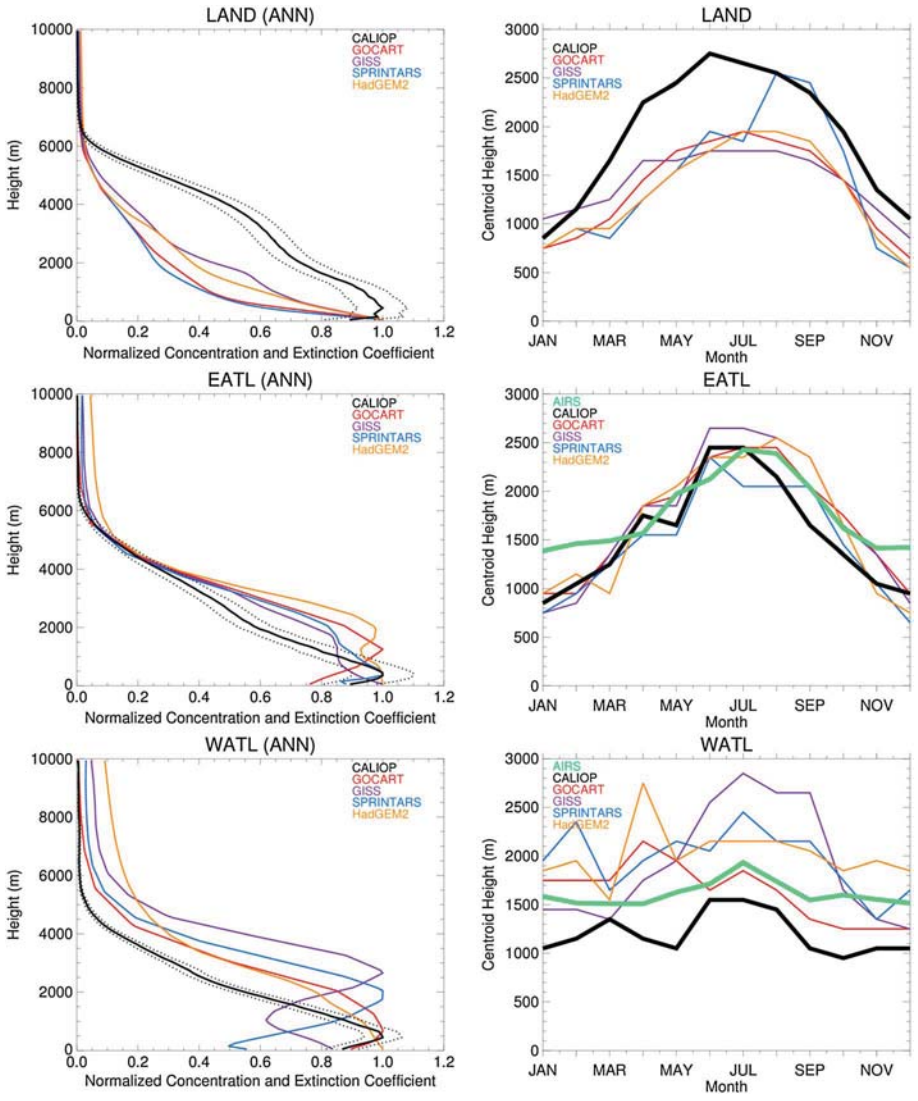

Figure 6. (left) Normalized annual mean (ANN) vertical profiles of dust concentrations. Dotted lines are the standard deviation of CALIOP data. (right) Monthly mean centroid height over land (17°W–30°E) and the Atlantic Ocean (90°W–17°W) from the models simulated for 2006. Ocean is divided to the east (EATL) and west (WATL) centered at 50°W. No data are available for ECHAM5. Normalized extinction efficient and centroid height of dust by CALIOP are averaged from 2007 up to 2009. Centroid height of dust by AIRS is averaged from 2004 up to 2008.

and outflow locations, Banizoumbou and Cape Verde, only appears in GOCART and GISS_CS. The observed coarse-mode AOD accounts for about 90% of the AOD at the North African AERONET stations and about 70% at La Parguera, indicating that dust is a dominant aerosol type there, but the DOD fraction can be much lower in some of the models, as will be shown in section 4.

3.4. Vertical Distribution of Dust

The vertical profiles of modeled dust are compared with the profile of dust extinction from CALIOP over land and ocean for 2007–2009 (i.e., Figure 6 (left)). Although the modeled dust extinction coefficient is not available in the AeroCom database, three-dimensional dust mass concentration is available only for 2006 except for ECHAM5, whereas the first full year of CALIOP data is 2007. Our analysis of GOCART simulations suggests that the shape of the dust mass concentration profile is similar to that of extinction. Therefore, here we compare the normalized vertical profiles of dust mass concentration from models for 2006 with the normalized dust extinction from CALIOP averaged for 2007–2009, both normalized to their respective

maximum values. Although the years are not the same between models and CALIOP, the general characteristics of regional statistics should be robust. These vertical profiles are averaged over land, the eastern Atlantic (EATL, 50°W–17°W), and the western Atlantic (WATL, 90°W–50°W).

Over land, the models show an exponential decay from surface to 6 km, which is much faster than the CALIOP data do. Over EATL, the models show that dust is lifted to higher altitudes, with a peak at 1000–2000 m, in contrast with the CALIOP data that have a maximum at 500 m and a faster decay with altitude compared to over land. The vertical shape in EATL is similar to that in WATL from CALIOP data, although it is slightly more extended in the vertical in EATL. However, the vertical distribution from the models can be quite different: a large spread of the peak layers' altitude is simulated over WATL due to the differences in vertical advection and dry and wet removal during transport. The large differences in vertical distribution between models and CALIOP are similar to those based on the AeroCom phase I model intercomparison study [*Koffi et al*., 2012]. Note that from east to west, the peak altitude shifts in different directions vertically among the models, i.e., altitudes from GISS and SPRINTARS are higher in WATL than in EATL, whereas those in GOCART and HadGEM2 are lower. The vertical distributions of CALIOP and the models are more extended during summer than winter in both the LAND and OCEAN domains (not shown but discussed with regard to the vertical distribution AOD centroid next).

The monthly dust centroid heights for CALIOP AOD and four models are calculated over each region (Figure 6 (right)). In addition, AIRS provides an independent AOD centroid height over ocean [*Peyridieu et al*., 2010, 2013]. The centroid height is the center elevation in a vertical profile of mass or optical extinction; thus, it provides useful information on the vertical distribution of dust. Over LAND, the CALIOP AOD centroid height shows clear and large seasonality, with summer high (2500–2800 m) and winter low (900–1200 m) centroid elevations. Over EATL, both CALIOP and AIRS also show strong centroid height seasonality, also with summer high (2200 ~ 2500 m) and winter low, although in winter the centroid height from CALIOP (900 m) is about 500 m lower than that from AIRS (~1400 m). Over WATL, the seasonality is much weaker, with the centroid heights in the range of 1000 ~ 1500 m for CALIOP, consistently lower than AIRS by 100–700 m. The strong seasonality of dust horizontal and vertical distributions over the Atlantic Ocean is also found in several previous studies using CALIOP [*Huang et al*., 2010; *Adams et al*., 2012]. It is worth noting that there is some difference in seasonality between CALIOP and AIRS, i.e., the summer peak for CALIOP (June) is 1 month earlier than for AIRS (July) in both EATL and WATL domains. Considerable differences in the CALIOP active sensor, visible NIR, and the AIRS passive, thermal IR measurements techniques, and their respective sensitivities to aerosol composition and size, along with sampling differences, can account for at least some of the apparent discrepancies.

The models show seasonal patterns similar to the observations over LAND and EATL except SPRINTARS over LAND, but they display a lower centroid height over LAND than CALIOP, especially during summer (~1 km lower). The agreement is much better over EATL, with model-observation differences within 500 m. Over WATL, the centroid heights among the models have much greater spread than for other regions; all of them are higher than the centroid height from CALIOP (by up to 1.5 km) and most of them higher than AIRS. Similar to CALIOP and AIRS, most models also have much weaker centroid height seasonal variation over WATL than over other regions, except the GISS model. The large differences in the centroid heights among models and between models and observations over the WATL reveal the model uncertainties in the height of long-range transport and the lifetime of dust plumes from Northern Africa to the western Atlantic.

4. Comparisons of Model's Emission and Physical/Optical Parameters

The comparisons shown in the previous section reveal substantial differences among the models in DOD and its spatial distribution, even over the source regions. Here we examine several fundamental parameters that may help diagnose the large diversities among the models. Figure 7 compares the dust emissions from the models. Note that ECHAM5 has the lowest mass emission range because it only considers smaller sizes in its modal approach (see Table 1). GOCART and SPRINTARS have the same maximum size of 10 μm (radius), but GOCART emissions are a factor of 2 larger than SPRINTARS. GISS and HadGEM2 have a maximum size larger than 10 μm, but their emissions are lower than GOCART (see Table 3). All models show dust emission "hot spots" such as Bodélé (18°E, 17°N) and Western Africa between (0–17°W, 15°N–30°N). GOCART, GISS, and

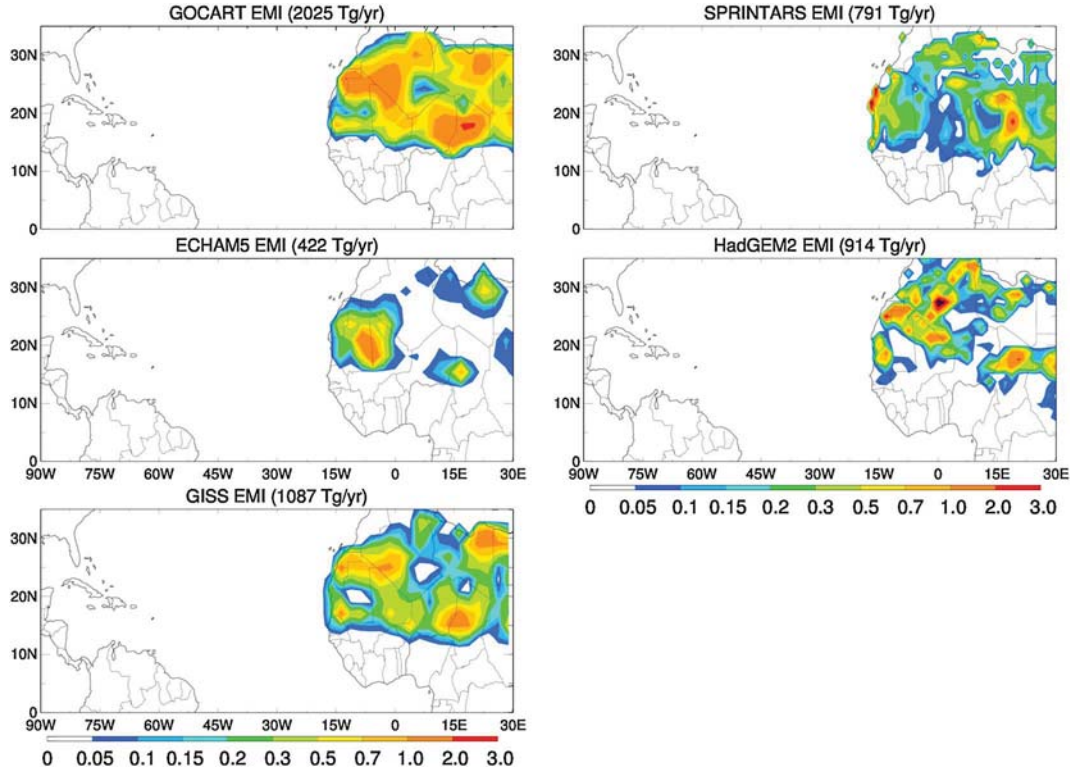

Figure 7. Mean dust emissions averaged over 2000–2005 from models. Color contour unit is in kg m^{-2} s^{-1}.

SPRINTARS cover broader source areas than ECHAM5 and HadGEM2. The domain-averaged dust emission differs by a factor of five among models, from 422 Tg yr^{-1} in ECHAM5 to 2025 Tg yr^{-1} in GOCART. Overall, the AOD and DOD spatial patterns over land (Figures 1 and 2) from the models generally follow the same emissions pattern.

We further compare three physical and optical parameters in the models: f_{WET}, the fraction of wet deposition to total deposition (or ratio of WET to DEP, where DEP = DRY + WET); loss frequency (LF), i.e., the ratio of DEP to LOAD or inverse of dust lifetime; and the dust mass extinction efficiency (MEE), i.e., the ratio of DOD to LOAD (Figure 8). Descriptions of these parameters and the mean values for each region are summarized in Table 3.

During long-range transport, aerosol loading and LF are determined by advection and deposition. The range of the annual LF domain mean among the models is between 0.28 and 0.37 day^{-1} (Figure 8a). Noticeable differences appear in the spatial distributions. For example, SPRINTARS and HadGEM2 show high LF (>0.9 day^{-1}) over Northern Africa, indicating that dust aerosols are quickly removed before being transported out. It is worth noting that GISS and ECHAM5 show high LF in the western Atlantic but much lower over Northern Africa. Loss frequency is mainly controlled by the DEP efficiency, where DEP = DRY + WET. Since each model has different DRY and WET parameterizations, DRY and WET efficiency is model dependent, and the loss frequency distribution is also highly model dependent, determined by the way the model handles DRY and WET in the dust budget, and DRY loss is also quite dependent on particle vertical distribution and to some extent on particle size. Our analysis indicates that the higher WET in GISS is related to the highly efficient WET process (i.e., larger f_{WET} in GISS than other models in Figure 8b), whereas the internal mixing assumption in ECHAM5 (which is the modal model) explains the faster removal of smaller particles over the western Atlantic Ocean. The LF also indicates that ECHAM5 has very little dust loss over the source regions. GOCART shows relatively moderate values over both land and ocean, so dust is removed over land and ocean with about the same efficiency.

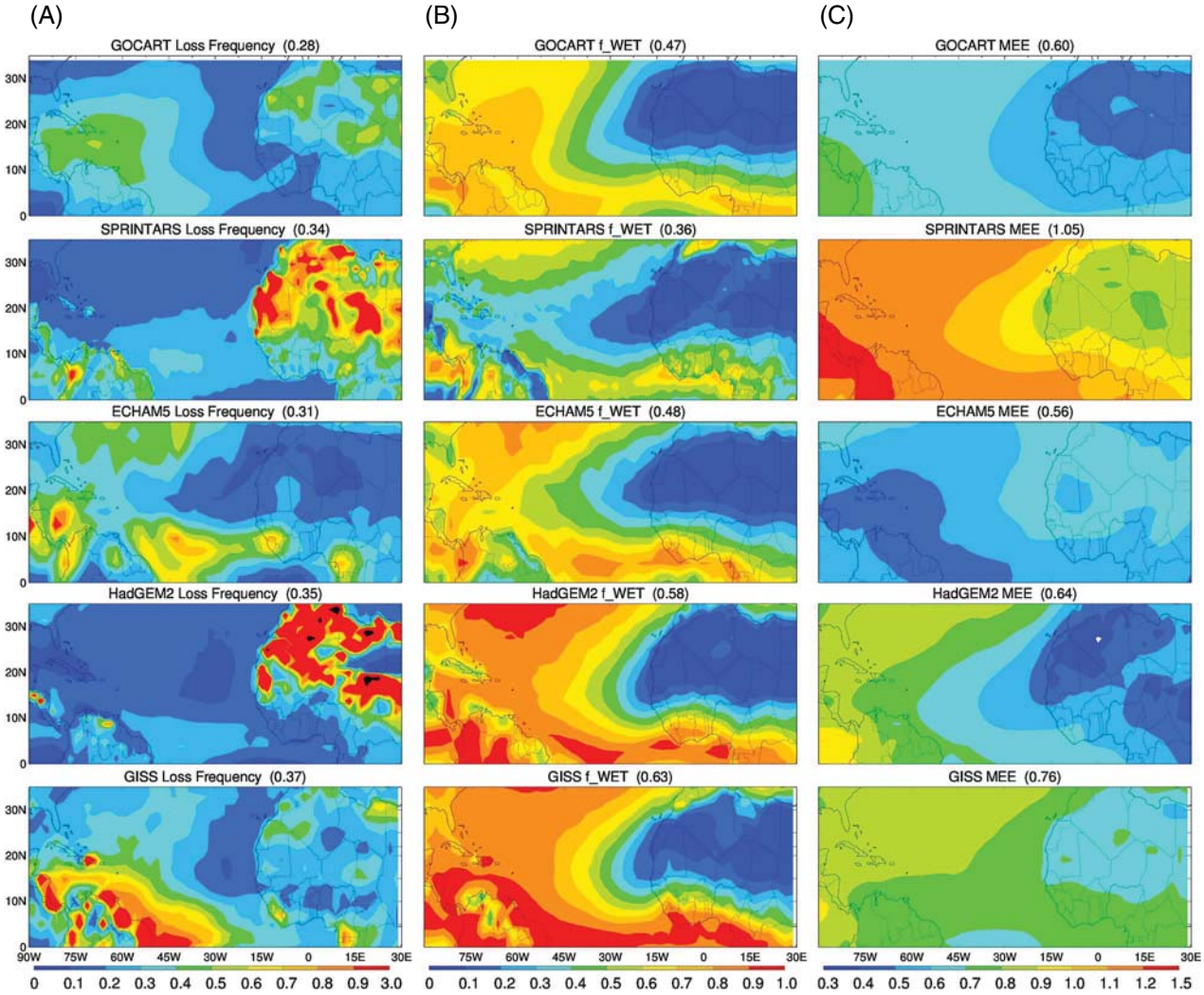

Figure 8. Map of loss frequency, f_{WET}, and MEE for dust averaged over 2000–2005 from models. (a) Loss frequency is the ratio of total removal rate to LOAD (day^{-1}), (b) f_{WET} is the fraction of wet removal in total removal, and (c) MEE is dust mass extinction efficiency at 550 nm (m^2 g^{-1}) (also see Table 3).

The distributions of the fraction of WET over total deposition (DEP), f_{WET}, are compared between models in Figure 8b. Over the Sahara desert and eastern Atlantic near the coast (east of 30°W), all the models give a consistent pattern with f_{WET} of less than 0.3 due to the dominant role of gravitational settling and aerodynamic dry deposition (collectively as DRY). Over the Atlantic Ocean west of 30°W, f_{WET} is substantially higher due to the dust removal via wet deposition, with the highest f_{WET} in GISS and the lowest in SPRINTARS. Overall, f_{WET} differs by a factor of 2 among the models, ranging from 0.36 (SPRINTARS) to 0.63 (GISS).

Wet deposition is controlled primarily by precipitation, cloud cover, precipitation type, vertical profile of aerosol and cloud, and aerosol size distribution. Among them, different input meteorology data between models are another major source of the uncertainty in wet deposition, affecting the simulated distribution of dust. The annual mean precipitation differences (kg m^{-2} d^{-1}) among the models are as large as 46% (2.80 in HadGEM2 and 4.10 in GOCART) (Figure S3). The models also show different seasonal variation, i.e., the highest and lowest precipitations (kg m^{-2} d^{-1}) appear in GISS (2.70) and ECHAM5 (1.55) during winter, whereas in GOCART (5.22) and SPRINTARS (3.25), they appear during summer. The dry deposition efficiency, which is defined as the ratio of DRY to LOAD, is model dependent, with the difference up to 30%.

Several assumptions in physical (e.g., density and size distribution) and optical properties (e.g., refractive indices) are used to calculate the mass extinction efficiency (MEE, m^2 g^{-1}) that converts dust mass to dust

extinction and optical depth. Considering the low hygroscopic nature of dust, we diagnostically derived a column-averaged dust MEE as the ratio of DOD to LOAD for different models. Note that the gradient in MEE of a model indicates the differences in the particle size distribution, e.g., MEE is higher for the fine-mode particles than the coarse-mode particles. In addition, different dust size ranges in different models also cause differences in MEE. The range of the domain mean dust MEE ($m^2\ g^{-1}$) among the models is from 0.56 (ECHAM5) to 1.05 (SPRINTARS) (Figure 8c). The range of dust MEE is model dependent (GOCART 0.4–0.8, GISS 0.6–1.0, SPRINTARS 0.7–1.5, ECHAM5 0.4–0.7, and HadGEM2 0.3–1.0). Most models show that dust MEE is lower over source regions than over downwind regions, which is consistent with a notion that the dust particle sizes are larger near the sources, and smaller particles, having higher MEE, are more efficiently transported away from the sources. In contrast, the ECHAM5 model shows higher MEE over land than over ocean. The evolution of MEE in the course of long-range transport is not well established from an observational standpoint. A previous study adopted a mass-specific extinction coefficient for Saharan dust from observational data that varies between 0.45 and 0.65 ($m^2\ g^{-1}$) during long-range transport [*Ansmann et al*., 2012], but another field measurement study found only negligible changes in dust size distribution based on dust sampled between the west coast of North Africa and Puerto Rico during July 2000 [*Maring et al*., 2003]. Hence, the observations do not provide a strong constraint on the models in the present study. Qualitatively, the GOCART and GISS models show less variation of MEE across the ocean.

We calculate model diversity (Table 3), which is defined as the ratio of the standard deviation of the model results to the multimodel mean [*Textor et al*., 2006]. Over the domain, diversity for the mass-related parameters (i.e., EMI, LOAD, DRY, and WET) is in the range of 59–69%, and for the optical parameters (i.e., AOD and DOD), it is in the range of 38–59%. For the other optical and physical parameters the diversity is in the range of 11–39%. Among the parameters in Table 3, LOAD, DOD, AOD, and LF have higher diversities over land (75%, 66%, 50%, and 44%, respectively) than over ocean (57%, 45%, 34%, and 37%, respectively). Furthermore, the diversity of optical and physical parameters is somewhat higher over either land (15–44%) or ocean (23–50%) than that over the whole domain (11–39%).

5. Discussion

The intermodel comparisons of dust simulations over North Africa and the North Atlantic shown in the previous sections have revealed significant differences among the models, despite some common features. Because similar comparisons were conducted with the AeroCom I models [*Textor et al*., 2006; *Kinne et al*., 2006; *Huneeus et al*., 2011], it is interesting to assess how the intermodel diversities have evolved since then, although the participating models and study domains/time periods are different between the previous studies and this work. Overall, the diversities of the mass budget terms of EMI, LOAD, DRY, and WET in AeroCom I models on "global scale" are 49–60%, 38–40%, 54%, and 97%, respectively, whereas in this "regional-scale" study they still remain largely diversified at 57%, 69%, 59%, and 61%, respectively. Model diversities of optical properties of DOD and MEE in the present study are 59% and 27%, respectively, compared to 38–44% and 38–45% in AeroCom I. In addition, a recent study has shown that the difference of dust wet deposition fraction (i.e., f_{WET}) between observations and the AeroCom phase I models at a few sites in Florida can be as large as a factor of 30 while models underestimate the observation. The f_{WET} values over Florida from the AeroCom II models in this study are similar to those from the AeroCom I models [*Huneeus et al*., 2011]; therefore, similar data-model discrepancies are likely. Although the spatial and temporal differences between this and previous studies may contribute to the differences between AeroCom I and AeroCom II results, the large intermodel diversities from the present study in the most important dust region indicate that, in general, little progress has been made since AeroCom I in dust modeling. The difficulty in making significant progress is partly due to the lack of observational constraints on some key physical and optical processes, such as emission, loss frequency, and mass extinction efficiency, to evaluate the model processes and parameters in order to make improvements. Among the available data sets, the derived DOD has much larger error and uncertainties than measured/retrieved AOD, and the surface dust deposition measurements are extremely sparse. It is highly desirable to have more ground-based stations to monitor dust concentrations and deposition with size distributions, as suggested by *Huneeus et al*. [2011].

When evaluating model results with the remote sensing data from satellites and AERONET, it would be most appropriate to use the clear-sky calculations from the models since the satellite and AERONET data are only available under the clear-sky conditions. However, most model-data comparison studies have been using the

AOD simulated under all-sky conditions because the models do not usually output the clear-sky results. The GISS model in the present work has shown substantial differences between all-sky and clear-sky AOD simulations such that the all-sky AOD can be as much as 50% higher than the clear-sky AOD in our study domain (mostly due to the growth of hygroscopic aerosols), suggesting that it is inappropriate to use the all-sky model results to compare with clear-sky observations from satellites. On the other hand, for DOD the difference is negligible because the dust is expected to be mostly hydrophobic.

Even though it is still challenging to use observations to constrain each physical process and optical property in dust modeling, we should take steps to improve the models with information from the available observations. Our study suggests that the dust source locations and emission amounts can be constrained by the satellite and ground-based observations of aerosol distribution patterns and magnitudes over the North African desert area, the removal rates across the North Atlantic Ocean can be improved based on the satellite-observed longitudinal gradient and the surface concentrations at the source and receptor locations, and the parameters determining the vertical profiles (such as convective transport and scavenging efficiency) can be optimized based on the lidar measurements. With more systematic, concerted observations available in the future and the increasing interest in understanding dust effects on the environment, more significant progresses on dust modeling will take place.

It is worth noting that the precipitation fields are different among models. Although the models agree well for extremely low precipitation over land and high precipitation over ocean, the precipitation rate can differ by a factor of about 2, in annual mean, among the models (i.e., 2.8–4.1 kg m^{-2} d^{-1}) (Figure S3). Such large differences in precipitation suggest that diversity in wet removal rates between models is inevitable, even with the same wet removal parameterization. The same applies to the emission processes, as the wind fields are model dependent.

Although DOD data derived from satellite remote sensing have provided unique insights into the general distribution and contribution of the transatlantic dust from North Africa, the DOD retrievals are subject to larger uncertainties than AOD. Also, coarse-mode AOD in AERONET and MODIS might be affected by both dust and sea salt at remote oceanic sites, such as La Parguera. Whereas next generation instruments would be required to substantially improve dust remote sensing from space, it would be helpful to fully explore the dust measurement capabilities of existing satellites through multisensor measurement synergy [*Yu et al.*, 2013].

6. Summary

We have evaluated the five AeroCom II global model simulations of dust aerosols over North Africa and the North Atlantic Ocean by comparing the model-simulated spatial and temporal distributions of total and dust aerosols with a suite of satellite remote sensing data and with AERONET Sun photometer measurements. We evaluated the following quantities: (1) AOD and DOD over land, ocean, and the entire study area within the domain, (2) the longitudinal gradient of AOD and DOD from the dust source regions of North Africa to the western North Atlantic, (3) the seasonal variations of AOD and DOD, and (4) the vertical distributions of dust aerosols. We have also compared several key quantities, including dust emission, dry and wet deposition, loss frequency (inverse of lifetime), and mass extinction efficiencies among the models, to help diagnose the reasons for the diversities of model-simulated DOD.

Data from the MODIS, MISR, and SeaWiFS satellite instruments show general agreement in the magnitude, seasonality, and spatial distribution pattern of AOD. On multiyear and area-averaged basis, AOD over land is 0.33–0.36, which is approximately twice of that over ocean. DODs derived from MODIS corrected fine-mode fraction and from MISR nonspherical fraction over ocean consistently show values of 0.10–0.12, contributing about 55% of AOD over the ocean domain. On the other hand, large differences are found between models and satellite data as well as among the models themselves for both AOD and DOD, ranging from 400% lower to 200% higher than satellite data, with 30–60% intermodel diversity, and all model-simulated DODs are lower by 0.01–0.09 than the satellite-derived values over ocean. Across the Atlantic Ocean from east to west, satellite data indicate a 50% decrease of both AOD and DOD and a 0.1–0.2 decrease of f_{DOD}. In comparison, most models have a stronger east-west DOD gradient, with a faster decrease of f_{DOD} from the west coast of North Africa to the western North Atlantic by 0.3–0.6. These results suggest that dust removal in the models during the transatlantic transport may be too efficient.

With regard to seasonal variations, all the satellite data show a summer maximum and winter minimum AOD and a second AOD peak in March over both land and ocean. Over ocean, they also show a DOD peak in the summer. However, none of the models reproduce the seasonal AOD variations over land, although some capture them over ocean for both AOD and DOD. Compared with the seasonal cycles and interannual variations of AOD over eight AERONET sites within the study domain, the model skills vary with location, the correlation coefficient ranges from 0 to 0.95, the bias ranges from 0.28 to 1.73, and the root-mean-square error ranges from 0.04 to 0.43.

The shapes of the dust vertical profiles from all models show much faster decrease with altitude over North Africa compared to CALIOP lidar. On the other hand, all modeled dust profiles are more vertically dispersed than the CALIOP data over the western North Atlantic. The resulting dust centroid height from the models is 0–1000 m lower than that from CALIOP over North Africa but 100–1400 m higher over the western North Atlantic, depending on season and model, with the largest discrepancies occurring in summer. The only region where models and CALIOP agree on the dust vertical extent to within 500 m is in the eastern North Atlantic. Comparisons with the dust centroid height from AIRS over ocean yield similar conclusions, although the centroid height from AIRS is a few hundred meters higher than that from CALIOP. The largest discrepancy between CALIOP and AIRS, between models and observations, and among the models is over the western North Atlantic, where the dust has traveled long distance from the source regions, highlighting the difficulties not only in model simulation of dust transport and associated processes but possibly also in satellite retrievals of dust vertical shape when the loading is lower.

We have compared four key parameters in five global models, including dust emission, loss frequency (LF), fraction of dust loss by wet deposition (f_{WET}), and dust mass extinction efficiency (MEE), to diagnose the intermodel differences of simulated dust loading and distributions. Although the dust emission is an "extensive property," depending on the number of dust bins and size ranges in each model, the latter three parameters can be considered as "intensive properties," associated with the model processes. Essentially, models differ by a factor of 5 in dust emission, with a diversity value of 57%. Although the intensive properties agree better among the models on domain average, with diversity values of 11%, 21%, and 27% for LF, f_{WET}, and MEE, respectively, they show significant spatial pattern disparities that reflect large differences in the treatment of dry and wet removal processes and in assumed optical properties. These parameters, however, are difficult to evaluate because of limitations in available observations.

This study has clearly revealed the challenges in simulating atmospheric dust aerosols even in an area with relatively abundant observations and little interference from other aerosol types. To move forward with model improvements, carefully planned systematic observations aimed at observing dust atmospheric processes during each step of dust life cycle are highly desirable.

Acknowledgments

This work is supported by NASA Modeling, Analysis and Prediction (MAP) and EOS Programs. H.Y. acknowledges the NASA support via NNX11AH66G. K.T. and S.E.B. were supported by NASA-MAP (NASA award: NNX09AK32G) and B.K. by the European Commission (AA AMITO 070307/ENV/2012/636596/C3). We would like to thank the MODIS, MISR, SeaWiFS, CALIOP, and AERONET teams for the data used in this study. Resources supporting this work were provided by the NASA High-End Computing (HEC) Program through the NASA Center for Climate Simulation (NCCS) at Goddard Space Flight Center.

References

Adams, A. M., J. M. Prospero, and C. Zhang (2012), *CALIPSO*-derived three-dimensional structure of aerosol over the Atlantic basin and adjacent continents, *J. Clim.*, *25*, 6862–6879.

Ansmann, A., P. Seifert, M. Tesche, and U. Wandinger (2012), Profiling of fine and coarse particle mass: Case studies of Saharan dust and Eyjafjallajökull/Grimsvötn volcanic plumes, *Atmos. Chem. Phys.*, *12*, 9399–9415.

Bauer, S. E., and D. Koch (2005), Impact of heterogeneous sulfate formation at mineral dust surfaces on aerosol loads and radiative forcing in the Goddard Institute for Space Studies general circulation model, *J. Geophys. Res.*, *110*, D17202, doi:10.1029/2005JD005870.

Bauer, S. E., M. I. Mishchenko, A. A. Lacis, S. Zhang, J. Perlwitz, and S. M. Metzger (2007), Do sulfate and nitrate coatings on mineral dust have important effects on radiative properties and climate modeling?, *J. Geophys. Res.*, *112*, D06307, doi:10.1029/2005JD006977.

Bellouin, N., J. Rae, A. Jones, C. Johnson, J. Haywood, and O. Boucher (2011), Aerosol forcing in the Climate Model Intercomparison Project (CMIP5) simulations by HadGEM2-ES and the role of ammonium nitrate, *J. Geophys. Res.*, *116*, D20206, doi:10.1029/2011JD016074.

Carlson, T. N., and J. M. Prospero (1972), The large-scale movement of Saharan air outbreaks of the northern equatorial Atlantic, *J. Appl. Meteorol.*, *11*, 283–297.

Chin, M., et al. (2002), Tropospheric aerosol optical thickness from the GOCART model and comparisons with satellite and Sun photometer measurements, *J. Atmos. Sci.*, *59*, 461–483.

Chin, M., T. Diehl, O. Dubovik, T. F. Eck, B. N. Holben, A. Sinyuk, and D. G. Streets (2009), Light absorption by pollution, dust and biomass burning aerosols: A global model study and evaluation with AERONET data, *Ann. Geophys.*, *27*, 3439–3464.

Dubovik, O., A. Smirnov, B. N. Holben, M. D. King, Y. J. Kaufman, T. F. Eck, and I. Slutsker (2000), Accuracy assessments of aerosol optical properties retrieved from Aerosol Robotic Network (AERONET) Sun and sky radiance measurements, *J. Geophys. Res.*, *105*, 9791–9806, doi:10.1029/2000JD900040.

Evan, A. T., A. K. Heidinger, R. Bennartz, V. Bennington, N. M. Mahowald, H. Corrada-Bravo, C. S. Velden, G. Myhre, and J. P. Kossin (2008), Ocean temperature forcing by aerosols across the Atlantic tropical cyclone development region, *Geochem. Geophys. Geosyt.*, *9*, Q05V04, doi:10.1029/2007GC001774.

Forster, P., et al. (2007), Changes in atmospheric constituents and in radiative forcing, in *Climate Change 2007: The Physical Science Basis, Contribution of Working Group I to the Fourth Assessment Report of the Intergovernmental Panel on Climate Change*, edited by S. Solomon et al., pp. 129–234, Cambridge Univ. Press, Cambridge, U. K.

Ginoux, P., et al. (2001), Sources and distributions of dust aerosols simulated with the GOCART model, *J. Geophys. Res.*, *106*(D17), 20,255–20,273, doi:10.1029/2000JD000053.

Ginoux, P., J. M. Prospero, O. Torres, and M. Chin (2004), Long-term simulation of global dust distribution with the GOCART model: Correlation with the North Atlantic Oscillation, *Environ. Modell. Software*, *19*, 113–128, doi:10.1016/S1364-8152(03)00114-2.

Guelle, W., Y. J. Balkanski, M. Schulz, B. Marticorena, G. Bergametti, C. Moulin, R. Arimoto, and K. D. Perry (2000), Modeling the atmospheric distribution of mineral aerosol: Comparison with ground measurements and satellite observations for yearly and synoptic timescales over the North Atlantic, *J. Geophys. Res.*, *105*, 1997–2012, doi:10.1029/1999JD901084.

Guo, Y., B. Tian, R. A. Kahn, O. Kalashnikova, S. Wong, and D. E. Waliser (2013), Tropical Atlantic dust and smoke aerosol variations related to the Madden-Julian Oscillation in MODIS and MISR observations, *J. Geophys. Res. Atmos.*, *118*, 4947–4963, doi:10.1002/jgrd.50409.

Haywood, J. M., P. Francis, S. Osborne, M. Glew, N. Loeb, E. Highwood, D. Tanre, G. Myhre, P. Formenti, and E. Hirst (2003), Radiative properties and direct radiative effect of Saharan dust measured by the C-130 aircraft during SHADE: 1. Solar spectrum, *J. Geophys. Res.*, *108*(D18), 8577, doi:10.1029/2002JD002687.

Holben, B. N., et al. (1998), AERONET—A federated instrument network and data archive for aerosol characterization, *Remote Sens. Environ.*, *66*, 1–16.

Hsu, N. C., S. C. Tsay, M. D. King, and J. R. Herman (2004), Aerosol properties over bright-reflecting source regions, *IEEE Trans. Geosci. Remote Sens.*, *42*(3), 557–569.

Hsu, N. C., et al. (2006), Deep blue retrievals of Asian aerosol properties during ACE-Asia, *IEEE Trans. Geosci. Remote Sens.*, *44*, 3180–3195.

Hsu, N. C., R. Gautam, A. M. Sayer, C. Bettenhausen, C. Li, M. J. Jeong, S.-C. Tsay, and B. N. Holben (2012), Global and regional trends of aerosol optical depth over land and ocean using SeaWiFS measurements from 1997 to 2010, *Atmos. Chem. Phys.*, *12*, 8037–8053.

Huang, J., C. Zhang, and J. M. Prospero (2010), African dust outbreaks: A satellite perspective of temporal and spatial variability over the tropical Atlantic Ocean, *J. Geophys. Res.*, *115*, D05202, doi:10.1029/2009JD012516.

Huneeus, N., et al. (2011), Global dust model intercomparison in AeroCom phase I, *Atmos. Chem. Phys.*, *11*, 7781–7816, doi:10.5194/acp-11-7781-2011.

Jickells, T. D., et al. (2005), Global iron connections between desert dust, ocean biogeochemistry, and climate, *Science*, *308*, 67–71.

Kahn, R. A., et al. (2009), MISR aerosol product attributes and statistical comparisons with MODIS, *IEEE Trans. Geosci. Rem. Sens.*, *47*(12), 4095–4114, doi:10.1109/TGRS.2009.2023115.

Kahn, R. A., B. J. Gaitley, M. J. Garay, D. J. Diner, T. Eck, A. Smirnov, and B. N. Holben (2010), Multiangle Imaging SpectroRadiometer global aerosol product assessment by comparison with the Aerosol Robotic Network, *J. Geophys. Res.*, *115*, D23209, doi: 10.1029/2010JD014601.

Kalashnikova, O. V., and R. A. Kahn (2006), Ability of multiangle remote sensing observations to identify and distinguish mineral dust types: Part 2. Sensitivity over dark water, *J. Geophys. Res.*, *111*, D11207, doi:10.1029/2005JD006756.

Kaufman, Y. J., I. Koren, L. A. Remer, D. Tanré, P. Ginoux, and S. Fan (2005), Dust transport and deposition observed from the Terra-Moderate Resolution Imaging Spectroradiometer (MODIS) spacecraft over the Atlantic Ocean, *J. Geophys. Res.*, *110*, D10S12, doi:10.1029/2003JD004436.

Kim, K.-M., W.-K. Lau, Y. C. Sud, and G. K. Walker (2010), Influence of aerosol-radiative forcings on the diurnal and seasonal cycles of rainfall over West Africa and Eastern Atlantic Ocean using GCM simulations, *Clim. Dyn.*, *11*, 115–126, doi:10.1007/s00382-010-0750-1.

Kinne, S., et al. (2006), An AeroCom initial assessment optical properties in aerosol component modules of global models, *Atmos. Chem. Phys.*, *6*, 1815–1834.

Koffi, B., et al. (2012), Application of the CALIOP layer product to evaluate the vertical distribution of aerosols estimated by global models: AeroCom phase I results, *J. Geophys. Res.*, *117*, D10201, doi:10.1029/2011JD016858.

Levy, R. C., L. A. Remer, R. G. Kleidman, S. Mattoo, C. Ichoku, R. Kahn, and T. F. Eck (2010), Global evaluation of the Collection 5 MODIS dark-target aerosol products over land, *Atmos. Chem. Phys.*, *10*(21), 10,399–10,420, doi:10.5194/acp-10-10399-2010.

Liu, D., Z. Wang, Z. Liu, D. Winker, and C. Trepte (2008), A height resolved global view of dust aerosols from the first year CALIPSO lidar measurements, *J. Geophys. Res.*, *113*, D16214, doi:10.1029/2007JD009776.

Maher, B. A., J. M. Prospero, D. Mackie, D. Gaiero, P. Hesse, and Y. Balkanski (2010), Global connections between aeolian dust, climate and ocean biogeochemistry at the present day and at the last glacial maximum, *Earth Sci. Rev.*, *99*(1–2), 61–97, doi:10.1016/j.earscirev.2009.12.001.

Mahowald, N. M. (2007), Anthropocene changes in desert area: Sensitivity to climate model predictions, *Geophys. Res. Lett.*, *34*, L18817, doi:10.1029/2007GL030472.

Mahowald, N. M., et al. (2010), Observed 20th century desert dust variability: Impact on climate and biogeochemistry, *Atmos. Chem. Phys.*, *10*, 10,875–10,893, doi:10.5194/acp-10-10875-2010.

Mahowald, N., S. Albani, J. F. Kok, S. Engelstader, R. Scanza, D. S. Ward, and M. G. Flanner (2013), The size distribution of desert dust aerosols and its impact on the Earth system, *Aeolian Res.*, doi:10.1016/j.aeolia.2013.09.002, in press.

Maring, H., D. L. Savoie, M. A. Izaguirre, and L. Custals (2003), Mineral dust aerosol size distribution change during atmospheric transport, *J. Geophys. Res.*, *108*(D19), 8592, doi:10.1029/2002JD002536.

Miller, R. L., et al. (2006), Mineral dust aerosols in the NASA Goddard Institute for Space Sciences ModelE atmospheric general circulation model, *J. Geophys. Res.*, *111*, D06208, doi:10.1029/2005JD005796.

Nowottnick, E., P. Colarco, R. Ferrare, G. Chen, S. Ismail, B. Anderson, and E. Browell (2010), Online simulations of mineral dust aerosol distributions: Comparisons to NAMMA observations and sensitivity to dust emission parameterization, *J. Geophys. Res.*, *115*, D03202, doi:10.1029/2009JD012692.

Omar, A., et al. (2009), The CALIPSO automated aerosol classification and lidar ratio selection algorithm, *J. Atmos. Oceanic Technol.*, *26*, 1994–2014, doi:10.1175/2009JTECHA1231.1.

Peyridieu, S., A. Chédin, D. Tanre, V. Capelle, C. Pierangelo, N. Lamquin, and R. Armante (2010), Saharan dust infrared optical depth and altitude retrieved from AIRS: A focus over North Atlantic—Comparisons to MODIS and CALIPSO, *Atmos. Chem. Phys.*, *10*, 1953–1967.

Peyridieu, S., et al. (2013), Characterisation of dust aerosols in the infrared from IASI and comparison with PARASOL, MODIS, MISR, CALIOP, and AERONET observations, *Atmos. Chem. Phys.*, *13*, 6065–6082.

Pierce, J. R., R. A. Kahn, M. R. Davis, and J. M. Comstock (2010), Detecting thin cirrus in Multiangle Imaging Spectroradiometer aerosol retrievals, *J. Geophys. Res.*, *115*, D08201, doi:10.1029/2009JD013019.

Pozzoli, L., I. Bey, S. Rast, M. G. Schultz, P. Stier, and J. Feichter (2008), Trace gas and aerosol interactions in the fully coupled model of aerosol-chemistry-climate ECHAM5-HAMMOZ: 2. Impact of heterogeneous chemistry on the global aerosol distributions, *J. Geophys. Res.*, *113*, D07309, doi:10.1029/2007JD009008.

Pozzoli, L., G. Janssens-Maenhout, T. Diehl, I. Bey, M. G. Schultz, J. Feichter, E. Vignati, and F. Dentener (2011), Re-analysis of tropospheric sulfate aerosol and ozone for the period 1980–2005 using the aerosol-chemistry-climate model ECHAM5-HAMMOZ, *Atmos. Chem. Phys.*, *11*, 9563–9594, doi:10.5194/acp-11-9563-2011.

Prospero, J. M. (1999), Long-term measurements of the transport of African mineral dust to the southeastern United States: Implications for regional air quality, *J. Geophys. Res.*, *104*, 15,917–15,928, doi:10.1029/1999JD900072.

Prospero, J. M., P. Ginoux, O. Torres, S. E. Nicholson, and T. E. Gill (2002), Environmental characterization of global sources of atmospheric soil dust identified with the NIMBUS 7 Total Ozone Mapping Spectrometer (TOMS) absorbing aerosol product, *Rev. Geophys.*, *40*(1), 1002, doi:10.1029/2000RG000095.

Prospero, J. M., W. M. Landing, and M. Schulz (2010), African dust deposition to Florida: Temporal and spatial variability and comparisons to models, *J. Geophys. Res.*, *115*, D13304, doi:10.1029/2009JD012773.

Ridley, D. A., C. L. Heald, and B. Ford (2012), North African dust export and deposition: A satellite and model perspective, *J. Geophys. Res.*, *117*, D02202, doi:10.1029/2011JD016794.

Sayer, A. M., N. C. Hsu, C. Bettenhausen, M.-J. Jeong, B. N. Holben, and J. Zhang (2012), Global and regional evaluation of over-land spectral aerosol optical depth retrievals from SeaWiFS, *Atmos. Meas. Tech.*, *5*, 1761–1778, doi:10.5194/amt-5-1761-2012.

Schulz, M., et al. (2006), Radiative forcing by aerosols as derived from the AeroCom present-day and pre-industrial simulations, *Atmos. Chem. Phys.*, *6*, 5225–5246.

Shao, Y., K.-H. Wyrwoll, A. Chappell, J. Huang, Z. Lin, G. H. McTainsh, M. Mikami, T. Y. Tanaka, X. Wang, and S. Yoon (2011), Dust cycle: An emerging core theme in Earth system science, *Aeolian Res.*, *2*(4), 181–204, doi:10.1016/j.aeolia.2011.02.001.

Stier, P., et al. (2005), The aerosol-climate model ECHAM5-HAM, *Atmos. Chem. Phys.*, *5*, 1125–1156.

Takemura, T., H. Okamoto, Y. Maruyama, A. Numaguti, A. Higurashi, and T. Nakajima (2000), Global three-dimensional simulation of aerosol optical thickness distribution of various origins, *J. Geophys. Res.*, *105*, 17,853–17,873, doi:10.1029/2000JD900265.

Takemura, T., T. Nozawa, S. Emori, T. Y. Nakajima, and T. Nakajima (2005), Simulation of climate response to aerosol direct and indirect effects with aerosol transport-radiation model, *J. Geophys. Res.*, *110*, D02202, doi:10.1029/2004JD005029.

Tegen, I., and I. Fung (1995), Contribution to the atmospheric mineral aerosol load from land surface modification, *J. Geophys. Res.*, *100*, 18,707–18,726, doi:10.1029/95JD02051.

Textor, C., et al. (2006), Analysis and quantification of the diversities of aerosol life cycles within AeroCom, *Atmos. Chem. Phys.*, *6*, 1777–1813.

Uno, I., K. Eguchi, K. Yumimoto, T. Takemura, A. Shimizu, M. Uematsu, Z. Liu, Z. Wang, Y. Hara, and N. Sugimoto (2009), Asian dust transported one full circuit around the globe, *Nat. Geosci.*, *2*, 557–560, doi:10.1038/ngeo583.

Vignati, E., J. Wilson, and P. Stier (2004), M7: An efficient size resolved aerosol microphysics module for large-scale aerosol transport models, *J. Geophys. Res.*, *109*, D22202, doi:10.1029/2003JD004485.

Wong, S., A. E. Dessler, N. M. Mahowald, P. R. Colarco, and A. da Silva (2008), Long-term variability in Saharan dust transport and its link to North Atlantic sea surface temperature, *Geophys. Res. Lett.*, *35*, L07812, doi:10.1029/2007GL032297.

Yu, H., M. Chin, L. A. Remer, R. G. Kleidman, N. Bellouin, H. Bian, and T. Diehl (2009), Variability of marine aerosol fine-mode fraction and estimates of anthropogenic aerosol component over cloud-free oceans from the Moderate Resolution Imaging Spectroradiometer (MODIS), *J. Geophys. Res.*, *114*, D10206, doi:10.1029/2008JD010648.

Yu, H., L. Remer, M. Chin, H. Bian, Q. Tan, T. Yuan, and Y. Zhang (2012), Aerosols from overseas rival domestic emissions over North America, *Science*, *337*, 566–569, doi:10.1126/science.1217576.

Yu, H., M. Chin, D. M. Winker, A. H. Omar, Z. Liu, C. Kittaka, and T. Diehl (2010), Global view of aerosol vertical distributions from CALIPSO lidar measurements and GOCART simulations: Regional and seasonal variations, *J. Geophys. Res.*, *115*, D00H30, doi:10.1029/2009JD013364.

Yu, H., L. A. Remer, R. A. Kahn, M. Chin, and Y. Zhang (2013), Satellite perspective of aerosol intercontinental transport: From qualitative tracking to quantitative characterization, *Atmos. Res.*, *124*, 73–100.

Zhao, C., X. Liu, L. R. Leung, B. Johnson, S. McFarlane, W. I. Gustafson Jr., J. D. Fast, and R. Easter (2010), The spatial distribution of mineral dust and its shortwave radiative forcing over North Africa: Modeling sensitivity to dust emissions and aerosol size treatments, *Atmos. Chem. Phys.*, *10*, 8821–8838.

Zhao, C., X. Liu, L. R. Leung, and S. Hagos (2011), Radiative impact of mineral dust on monsoon precipitation variability over West Africa, *Atmos. Chem. Phys.*, *11*, 1879–1893.

Zhao, C., S. Chen, L. R. Leung, Y. Qian, J. Kok, R. Zaveri, and J. Huang (2013), Uncertainty in modeling dust mass balance and radiative forcing from size parameterization, *Atmos. Chem. Phys.*, *13*, 10,733–10,753.

Zender, C. S., H. Bian, and D. Newman (2003), Mineral Dust Entrainment and Deposition (DEAD) model: Description and 1990s dust climatology, *J. Geophys. Res.*, *108*(D14), 4416, doi:10.1029/2002JD002775.